Angular velocity vector determination of spacecraft in flat-spin attitude states

Laurence D. J. Blacketer
Northern Space and Security Ltd.

20/08/2022

ABSTRACT

Knowledge of space object attitude state is required for range of different applications. One example is accurate modelling of forces such as solar radiation pressure and atmospheric drag, which are required for the most accurate predictions of an object's motion. Accurate information on space object attitude state can therefore be used to improve the accuracy of conjunction assessment and reentry analysis. Another example is active debris removal (ADR). For an ADR mission to interface with an object, such as with a robotic arm, the object's attitude state must be known. Additionally, it must be determined if the object's attitude state is beyond the capability of the ADR spacecraft to remove, such as due to the angular rotation rate being too high.

In the cases of inactive space objects that are unable to communicate information regarding their attitude state, the state must be determined using external observation data. Brightness verses time measurements collected using ground-based optical telescopes have proven to be a capable and cost-effective method for collecting this observation data.

This paper explores a technique for attitude determination of two classes of space object - rocket bodies and 'box-wing' satellites. In each case, the initial problem is constrained to inactive objects that exhibit highly periodic brightness data and the rotational states are assumed to be a 'flat-spin'. Angular velocity vectors are then determined using a brute force inverse modelling technique, whereby a real light curve is simulated using a synthetic light curve model in combination with an approximate object geometry. The final angular velocity solution is defined by the synthetic light curve that best-fits the real light curve data. The results show that this technique can be used to determine unique angular velocity vector solutions for both box-wing satellites and rocket bodies. This is achieved using approximate object geometry models, showing that high fidelity geometry models are not necessary, which greatly decreases computational complexity.

1. INTRODUCTION

Modern day Space Surveillance and Tracking capabilities maintain up-to-date orbital positioning data on the majority of space objects in Earth orbit with sizes of approximately 10 cm and greater. This tracking information is available publicly as Two Line Elements (TLE) through the Space-Track website (`Space-Track.org`). These TLEs are an incredibly valuable resource and are used in a wide range of academic and industrial applications. However, their relatively low accuracy can limit their usefulness. Information on space object attitude state is substantially less common, and no public repository of data exists that is comparable to Space-Track. Although this information may be possible to downlink from active spacecraft, in many cases it is not freely shared. Space object attitude state can be used for a range of different applications.

The first application is higher accuracy calculation of attitude dependent forces such as Solar Radiation Pressure and atmospheric drag. Depending on the orbital regime, these forces can have a significant effect on an object's orbital motion. Knowing the attitude state of a space object could therefore be used to benefit applications that require high-accuracy propagation, such as conjunction assessment and re-entry prediction.

Collision activity, particularly in Low Earth Orbit (LEO), has been identified as a possible mechanism by which the numbers of orbital debris fragments may continue to increase even in the absence of future launch activity [5]. Although long-term evolutionary modelling of the space debris environment is subject to a lot of uncertainty, the possible impact to our ability to utilise the near-Earth space environment is large. It is therefore widely agreed that collisions in LEO should be minimised. Improving the accuracy of conjunction analysis could play an important role in reducing LEO collision activity.

Another key result of long-term evolutionary space debris modelling research was that an active approach to space debris management may be required. This research found that removing high-risk objects from LEO may be able to mitigate collision-activity-driven-growth in the number of debris fragments [6, 4]. This is known as Active Debris Removal (ADR). A number of different ADR strategies have been proposed, but the most advanced by far is mechanical interface and de-orbit. This is typically performed by rendezvousing with the target and capturing it using a mechanical interface such as a robotic arm [9]. An effective ADR strategy will therefore rely heavily on having the capability to characterise an object's attitude state. This will begin with wide-scale attitude characterisation on a range of possible ADR targets for the target down-selection process. This is to ensure that the attitude states of the short-listed targets are within the capabilities of the ADR mission to capture. Up-to-date attitude information on these objects then needs to be maintained up until the ADR mission is launched, to ensure that the target remains viable.

In addition to general space situational awareness and ADR applications, interest in attitude information of space objects also extends to defence. Understanding the attitude of an unfriendly spacecraft may be useful for understanding the purpose and intent of a particular object.

In the cases where an object cannot downlink attitude information from onboard sensors, attitude characterisation must be performed using external observation data, typically from ground-based sensors. One such example is radar data. Large powerful radar installations such as the Tracking and Imaging Radar (TIRA) are capable of generating resolved imagery of large space objects in relatively low orbits [10]. This data is extremely powerful as it allows the attitude to be directly observed. However, radar installations such as TIRA are extremely expensive and small in number.

It is also possible to receive resolved optical imagery, but this is typically only possible from on-orbit sensors in close approach with the target object. This data is therefore also very rare.

An alternate data type that can be used to determine attitude information is optical light curves, which are defined as a high-cadence series of brightness over time measurements, typically in the visual band. Although a light curve is limited to the evolution of a single property in time, light curves can be collected in much larger numbers, across a wide range of objects, using relatively low cost hardware. Furthermore, optical light curves have a long history in determining rotation period of natural objects, such as asteroids [2], and are routinely used to make assessments of the tumble rate of artificial space objects [3]. However, the ability to perform full attitude determination reliably across the entire object population is an active area of research and a number of varied techniques have been proposed and tested [11, 7, 8].

This paper explores the technique of brute force inverse fitting. This technique uses a synthetic light curve simulation model to reproduce real light curve data and relies on a key assumption. It is assumed that when a match is found between the real and synthetic light curves, the attitude of the object in reality is the same as in the simulation model. The matching synthetic light curve is found using a brute force technique, whereby all possible combinations of parameters in some predefined input space are tested and the single set of parameters that produces the best-fit to the real data is identified. This is done through measuring a Root Mean Square Error (RMSE) between the two light curves.

To test and understand the performance of this technique, it was first applied to a best-case scenario — a spacecraft in a relatively fast 'flat spin'. In this scenario, the object is rotating around a single fixed rotation axis, which is aligned with the object's principle axis of inertia. Selecting objects with fast rotation periods — calculated through Phase Dispersion Minimisation (PDM) — ensures that a relatively short LEO light curve contains a reasonable number of full rotations. This paper focuses specifically on LEO objects, as large numbers of light curves are available from the Mini-Mega Tortora light curve database (`mmt.favor2.info`) [3]. Two classes of objects were considered, rocket bodies and 'box-wing' spacecraft. A box-wing is defined as an approximately cuboidal spacecraft bus with two deployable solar panels extending from opposite faces.

The most important input of a light curve simulation model when trying to replicate real world light curve data is the object geometry model. This paper intentionally uses simplistic geometry models for the rocket body and box-wing spacecraft. The objective of this work was therefore to show that a brute force inverse fitting approach can be used to determine the angular velocity vector for flat-spinning rocket bodies and box-wings, even when using simplistic geometrical representations of the target objects.

The work in this paper was conducted, in part, in an Astroscale UK led project to identify techniques for attitude state and attitude state evolution of possible ADR targets, which was funded by the National Space Technology Programme of the UK Government.

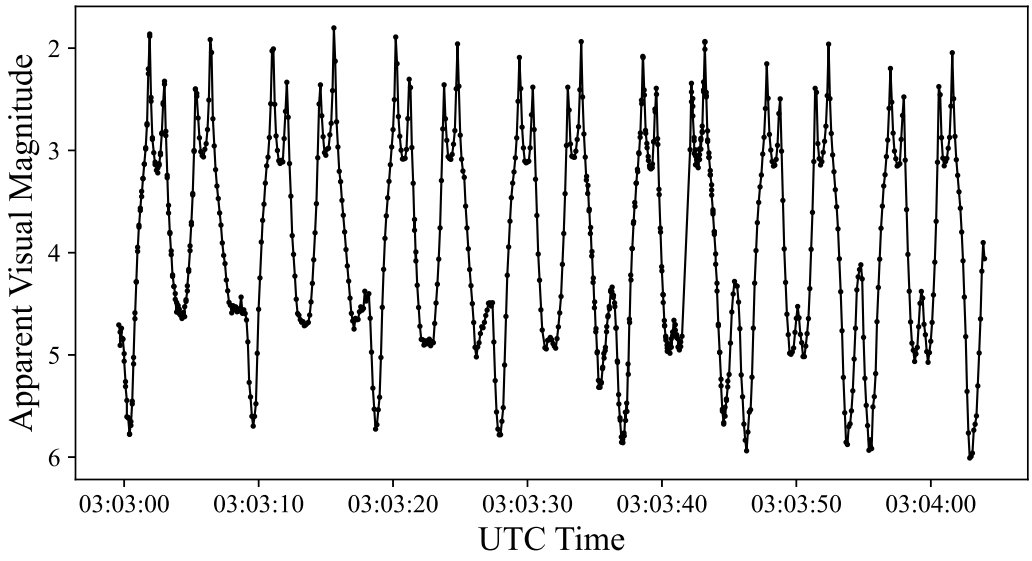

Fig. 1: The selected rocket body light curve. This light curve was collected on 11/02/2017 at 3:03:00 UTC by the MMT system and has a total duration of 64.4s. The object was a CZ-2D R/B, NORAD ID 41858.

2. METHODOLOGY

2.1 Object Selection

The first objective was to identify two objects, one rocket body and one box-wing, that would present suitable targets to test the proposed technique. In both cases, the objective was to find an object that exhibits highly structured periodic light curves. A highly structured periodic light curve is likely the result of a repeating sequence of clearly differentiable reflections from a repeating sequence of the same surfaces. This highly characteristic light curve shape maximises the uniqueness of the attitude solution, which provides a best-case scenario for the synthetic light curve model to successfully generate a unique match.

The objective in using a best-case scenario is to prove the validity of the technique. The vast amount of complexity and variation that is observed across the wide range of real world light curves can then be slowly introduced. Developing the technique in this way allows identification of the areas where the technique performs well, and the areas where the technique fails. These areas can then be focused on as the technique is developed further.

2.1.1 Rocket Body Light Curve

To select a suitable rocket body light curve, the MMT database was filtered to show only objects classified as rocket bodies with light curves flagged as periodic. This amounts to 456 objects. Applying an additional filter for only those objects with a PDM-determined period between 5–10 s results in a total of 46 objects. Limiting the rotation period to between these two values ensures that an MMT light curve, which is typically on the order of a minute in duration, contains a reasonable number of complete rotations.

The final selection of the target rocket body was performed by manually extracting the light curve that appeared to exhibit the most structure. This was the light curve shown in Fig. 1. The object is a CZ-2D rocket body (NORAD ID 41858), and the light curve was collected on 11/02/2017. Using PDM, the period of this light curve was determined to be 9.2 s.

To generate synthetic light curves for this object, a faceted geometry model was required. The objective in generating this geometry was to make it as simple as possible, whilst still being representative of the true shape. The model that was used is shown in Fig. 2. The geometry was generated with a total span in the z-axis of 8 m, and a radius of 3.35 m, taken from the ESA DISCOS database (`discosweb.esoc.esa.int`). In addition, each end was extended to a point

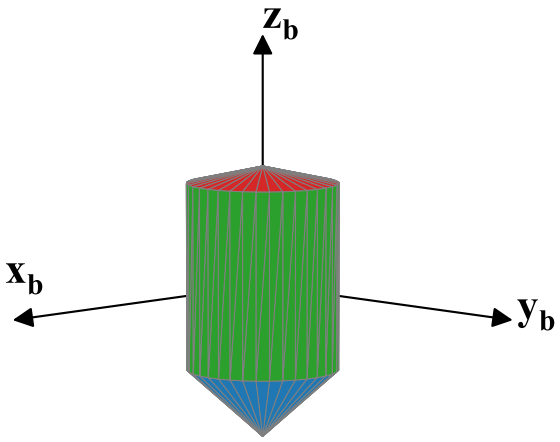

Fig. 2: The faceted object geometry used to represent a CZ-2D rocket body.

to better simulate reflections from the ends of the rocket body, where one end was extended further than the other, so to be representative of the rocket nozzle end.

The geometry model was broken down into three zones. The blue facets at the bottom of the geometry are the rocket nozzle end, the green facets are the main body and the red facets are the end without a rocket nozzle.

To simulate a flat-spin, the rotation axis for this object was set to be coincident with the x-body axis. The initial attitude state was described using the Euler angles, ψ, ϕ and θ, where ψ was initially applied to the x-body axis, then ϕ was applied to the y-body axis. This set the direction of rotation vector. Finally, θ was applied to the x-body axis to set the initial rotational state of the object. These rotations are applied in the object-centred orbital reference frame, which is defined by the Nadir and normal to the orbital plane vectors. The rotation vector is therefore stationary in the orbital frame and moving in the inertial frame.

2.1.2 Box Wing Light Curve

Selection of a suitable box-wing spacecraft was performed in a similar way as for the rocket body. The MMT database was filtered to show only objects classified as inactive satellites, with light curves flagged as periodic. This resulted in 95 objects. Of these 95, 27 were Globalstar satellites. In total, this resulted in 10960 periodic light curves of inactive Globalstar satellites. For this reason, combined with the fact that they have the desired box-wing shape, Globalstar satellites were selected. The specific object and light curve was selected by identifying a light curve with a period between 5 – 10 s, which exhibits the most highly structured shape.

The selected object was Globalstar M051, NORAD ID 25853, and the selected light curve was collected at 2:31:20 UTC on 14/02/2022. This light curve is shown in Fig. 3.

The geometry model that was used to represent the Globalstar spacecraft is shown in Fig. 4. This geometry model was generated using open source information on the approximate dimensions of the Globalstar bus and solar panels, and adheres to the objective of using a simplistic geometrical representation of the target objects.

The attitude motion was applied to this object in the same way as for the rocket body. The rotation axis was set to be coincident with the x-body axis and the initial attitude state was described using the Euler angles, ψ, ϕ and θ.

2.2 Synthetic Light Curve Model

The synthetic light curve model used in this paper consists of two primary components: the position data and transformations required to generate the illumination geometry and the brightness calculation itself. The position data is acquired from two sources. The first is TLEs and the Simple General Perturbations 4 (SGP4) orbital propagator, which are used to generate the object position at the times that a real light curve was generated. The second is the NASA HORIZONS database (`https://ssd.jpl.nasa.gov/?horizons`), which is used to generate position data

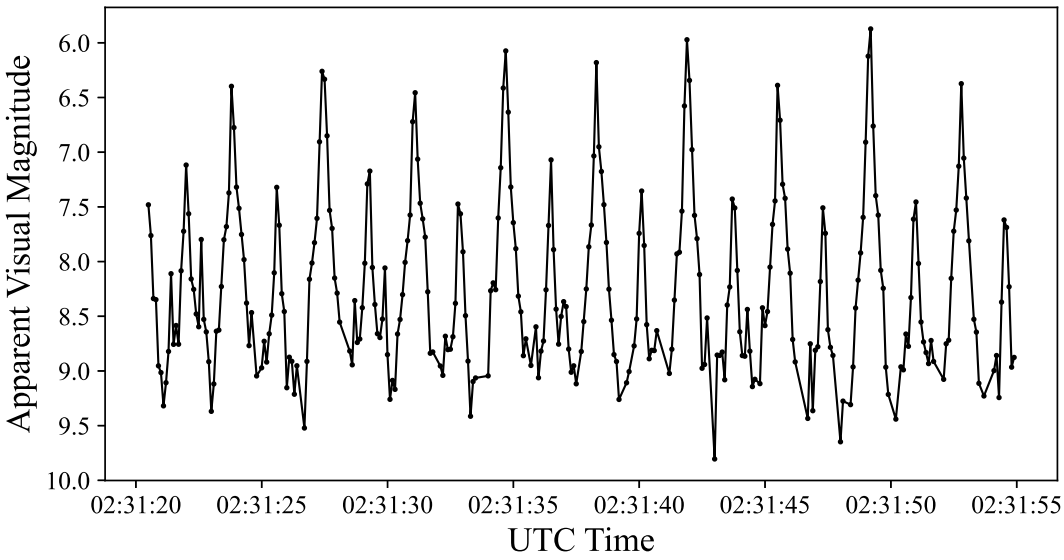

Fig. 3: The selected Globalstar M051 (NORAD ID 41858) light curve. This light curve was collected on 14/02/2022 at 2:31:20 UTC by the MMT system and has a total duration of 34.4s.

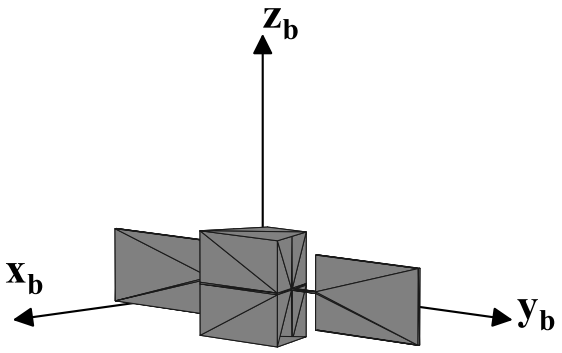

Fig. 4: A faceted object geometry for a Globalstar spacecraft.

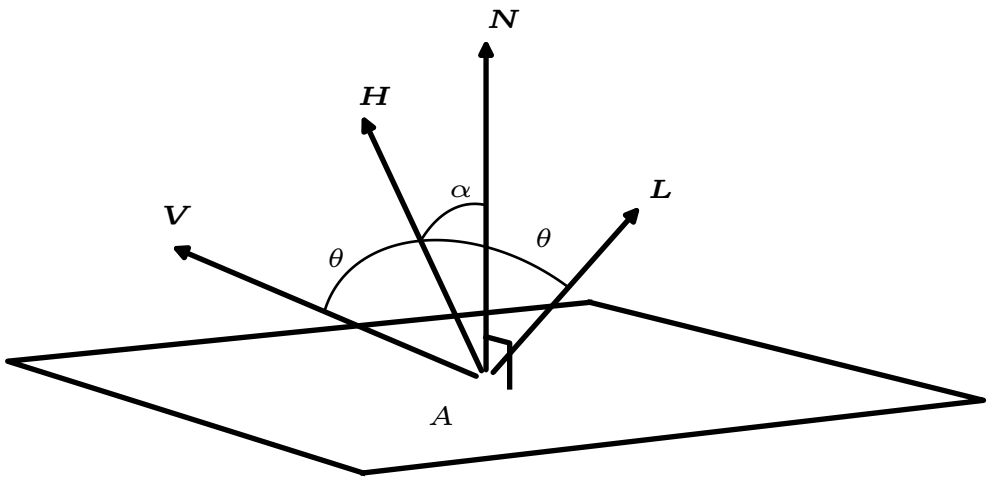

Fig. 5: The reflection geometry. **V** is the observation vector, **L** is the illumination vector and **H** is the angular bisector of these two vectors. **N** is the surface normal and A is the surface area.

for the Earth and the Sun. This data is combined and transformed into a body-fixed reference frame to generate the Sun-object-observer illumination geometry.

The next step is the brightness calculation. This is performed using a Bidirectional Reflectance Distribution Function (BRDF). This is a mathematical function that calculates the light reflected into a particular direction from some surface, due to illumination from some other direction. A number of different BRDFs exist which vary in their accuracy and complexity. This work makes use of the Cook-Torrence BRDF. This function was selected as it is well suited for modelling metallic surfaces, includes specular reflection — an important component of light curves of artificial space objects — and is relatively computationally inexpensive.

The Cook-Torrence BRDF is given by

$$B_i = (sR_s + dR_d)\pi A_i(\mathbf{N}_i \cdot \mathbf{L})(\mathbf{N}_i \cdot \mathbf{V}), \tag{1}$$

which calculates the ratio of incident to reflected flux, B_i, of some surface i, with an area of A_i, as a function of the specular reflectance R_s and the diffuse reflectance R_d, where s and d are the ratios of specular to diffuse reflection, with $s+d=1$. The vector properties **N**, **L** and **V** are the normal to the surface, the illumination vector and the observation vector respectively, as shown in Fig. 5. Also shown in Fig. 5 is **H**, the angular bisector of **L** and **V**.

The diffuse and specular reflectance are given by

$$R_d = \frac{\omega}{\pi}, \tag{2}$$

and

$$R_s = \frac{F}{\pi}\frac{DG}{(\mathbf{N}\cdot\mathbf{L})(\mathbf{N}\cdot\mathbf{V})}. \tag{3}$$

In these equations, ω is the diffuse albedo, F is surface reflectance, D is the facet slope function and G is the geometric attenuation factor. Calculating the facet slope function D, requires the definition of m (referred to in this paper as the 'roughness parameter'), a property which describes the roughness of the surface. Lower values for m correspond to a smoother surface, which results in a tighter distribution of the specular reflections. Additional information on the significance and calculation of these properties can be found in the original publication for the Cook-Torrence BRDF [1]. This work also adopts a simplification of this BRDF from Wetterer and Jah (2009) [11], where in the calculation of the surface reflectance, F_0, is set to be equal to ω.

Each face of the object geometry is therefore parametrised using three numbers, the diffuse ratio d (where $s = 1-d$), the diffuse albedo ω, and the roughness parameter m.

The brightness ratio calculated from Eqn. 1 is finally converted to an apparent visual magnitude value using

$$Vmag_{app} = -26.74 - 2.5\ log_{10}\left(\sum_{i=1}^{N_{facets}} \frac{B_i}{4\pi r^2}\right), \tag{4}$$

where -26.74 is the apparent visual magnitude of the Sun, N_{facets} is the total number of facets in the geometry model used to represent the object, r is the distance from the surface to the observer and B_i is the ratio of incident to reflected flux from Eqn. 1. A synthetic light curve is generated by evaluating Eqn. 4 at each time step of the simulation.

2.3 Brute Force Fitting

The brute force fitting was performed by testing all possible combinations of input parameters and extracting the single solution that minimised the difference between the real and synthetic light curves. The difference between the two light curves was quantified by measuring a Root Mean Square Error (RMSE) using the equation

$$RMSE = \sqrt{\frac{\sum_{i=1}^{n}(\hat{y}_i - y_i)}{n}}, \tag{5}$$

where n is the number of data points in the two light curves, $\hat{y}_i$ is the i^{th} value of the first light curve and y_i is the i^{th} value of the second light curve.

The parameters to be determined for each object were the Euler angles describing the initial attitude state at the beginning of the simulation, ψ, ϕ and θ, in addition to the three BRDF parameters, d, ω and m, for each face of the geometry model.

3. RESULTS

The results of this paper are those synthetic light curves of a box-wing spacecraft and a rocket body, that were identified as the closest match to real light curve data by minimising an RMSE measurement between the two signals.

3.1 Rocket Body Results

Fig. 6 shows the best-fitting synthetic light curve overlaid onto the real rocket body light curve. The colour of the light curve changes to indicate the level of involvement from the sides of the rocket body, relative to the two ends.

Initial brute force simulations for this object showed that individual BRDF parameters for each zone of the geometry (the sides and the two ends shown by the different colours in Fig. 2) were required in order to generate a synthetic light curve with a suitable match to the real data. This indicates that generating a match between the real and synthetic data is dependent on the differences in the reflective characteristics of the different zones of the object, rather than being only a function of the shape. The full set of inputs that needed to be determined, their ranges, and their final values, are shown in Tab. 1.

This result shows a strong agreement between the real and synthetic light curves. In addition to a match in the general positions of the peaks and troughs of the two signals, two key light curve features have been reproduced in the synthetic light curve. Firstly, the brightest reflections exhibit a double peak, where the one is brighter than the other. Two of these double peaks can be seen between 0 and 10 s in Fig. 6. The colour of the line shows that the brighter of the two peaks was due to reflections almost entirely from the side of the rocket body, whereas the slightly dimmer of the two peaks was due to reflection from one end of the rocket body. The second key feature is the difference in shape and brightness of the two troughs, which can be seen at approximately 5 s and 10 s in Fig. 6. Of these two troughs, one is a single trough whereas the other is a double trough. This is similar to what is seen in the real data. However, the shapes of the troughs in the real data change throughout the real light curve whereas those in the synthetic data do not. This is therefore the area of greatest disagreement between the two signals. Because factors such as changing illumination conditions are considered in the simulation model, this may suggest that the true attitude state has additional unmodeled components, such as motion in the orbital frame.

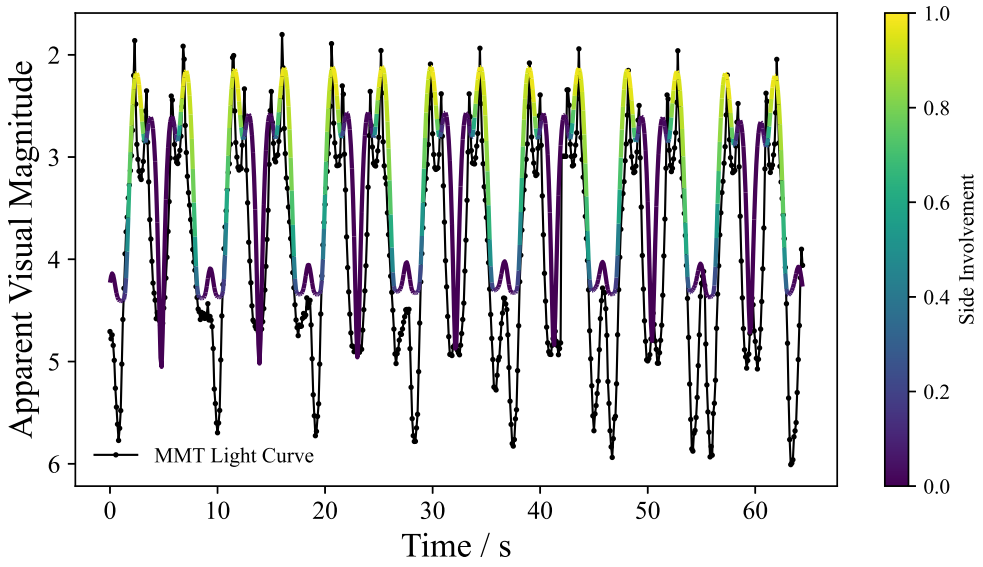

Fig. 6: The best-fitting synthetic light curve for the rocket body. The colour of the line indicates the proportion of the signal that was due to reflection from the side of the rocket body, rather than the two ends.

Table 1: Best-fitting parameters to generate a match between the real and synthetic light curves for the rocket body.

Property	Value	Testing Range	Step
ψ	350	0 - 350	10
ϕ	60	0 - 90	10
θ	0	0 - 350	10
ω_{top}	0.20	0.1 - 0.9	0.1
m_{top}	0.80	0.1 - 0.9	0.1
d_{top}	0.40	0.0 - 1.0	0.1
ω_{bottom}	0.40	0.1 - 0.9	0.1
m_{bottom}	0.40	0.1 - 0.9	0.1
d_{bottom}	0.70	0.0 - 1.0	0.1
ω_{side}	0.20	0.1 - 0.9	0.1
m_{side}	0.40	0.1 - 0.9	0.1
d_{side}	0.60	0.0 - 1.0	0.1

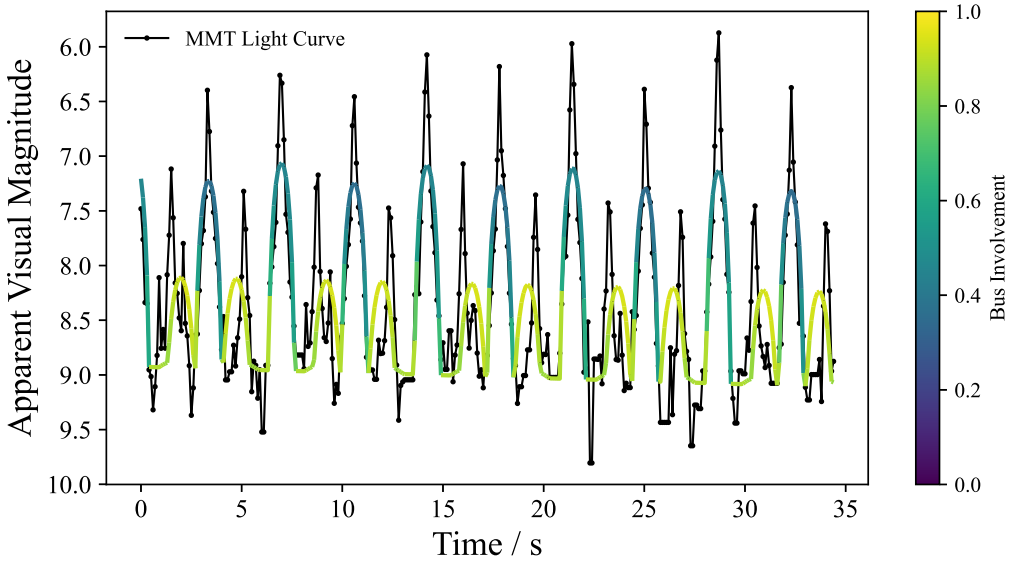

Fig. 7: The best-fitting synthetic light curve for the box-wing spacecraft. The colour of the line shows the proportion of the signal that was due to reflection from the spacecraft bus, rather than the solar panels.

3.2 Box-Wing Results

Fig. 7 shows the real light curve and the best fitting synthetic light curve for the box-wing spacecraft. The colour of the line indicates the proportion of the signal that was due to reflection from the spacecraft bus, relative to the solar panels.

Unlike for the rocket body, a reasonable match between the real and synthetic signals was achievable with a single set of BRDF parameters for all faces of the geometry model. Tab. 2 shows the set of parameters that were determined, their ranges, and the final values.

This result shows a good agreement between the real and synthetic signals. The synthetic light curve model has successfully matched the general positions of the peaks and troughs, and two distinct brightness peaks are correctly overlaid. The colour of the line shows that the brightest reflections in the synthetic light curve occur when bus involvement is low, showing that the cause of these reflections are the solar panels. In between each reflection from the solar panels is a reflection from the spacecraft bus, which coincides with the dimmer of the two brightness peaks in the real data. The fact that a single set of BRDF parameters have been used for the entirety of the geometry model shows that the match between the real and synthetic data is primarily a function of the object geometry. This is in contrast to the rocket body results, which required unique BRDF parameters for different zones of the geometry model. However, it is likely that the fit between the real and synthetic data could be improved by using unique BRDF parameters for the front and back of the solar panels, and for the bus.

Although the general fit between the real and synthetic data is good, there are features that do not perfectly overlay. For example, the dimmer of the two peaks that correspond to reflections from the bus do not perfectly match the real data, and none of the brightness peaks are as ‘sharp’ as in the real data. This is likely to be a result of differences between the geometry model used and the true shape. However, this is to be expected as the objective was to use a simple representative geometry, not to reproduce the true shape with a high level of detail.

4. CONCLUSIONS

In this paper a synthetic light curve model was used to reproduce a real light curve for a rocket body and a box-wing spacecraft. This was achieved using a brute force technique where all possible combinations of parameters in some predefined input space were tested. The best fitting set of input parameters was identified by minimising an RMSE measurement between the two signals. The results showed reasonable agreements between the real and synthetic data.

Table 2: Best-fitting parameters to generate a match between the real and synthetic light curves for the box-wing spacecraft.

Property	Value	Testing Range	Step
ψ	140	0 - 350	10
ϕ	50	0 - 90	10
θ	160	0 - 350	10
ω	0.9	0.1 - 0.9	0.1
m	0.2	0.1 - 0.9	0.1
d	0.4	0.0 - 1.0	0.1

For the rocket body, the synthetic light curve model was able to reproduce all of the key features in the real light curve. However, there were still some disagreements between the two signals, possibly caused by additional components to the attitude state beyond a stationary rotation vector in the orbital frame. It was found that to generate a suitable match, unique BRDF parameters were required for the three different zones of the geometry – the sides and the two ends. This is an indication that modelling the differences in the reflection characteristics of the different surfaces of the rocket body is an important factor in simulating their light curves.

For the box-wing spacecraft, the synthetic light curve model was capable of matching the sequence of bright and less bright reflections to the real data. However there was generally less structure in the light curve shape available to replicate compared to the rocket body. Fitting the box-wing light curve did not require unique BRDF parameters for different zones of the geometry. This indicates that, in contrast to the rocket body, the object shape plays a larger role in replicating the real data than the reflection characteristics of the i3ndividual surfaces.

A key objective of this paper was to show that a reasonable fit between real and synthetic light curves can be achieved when using simple geometrical representations of the target objects. This has been shown successfully. This is an important and valuable result as brute force fitting is highly computationally expensive and any introduction of additional geometrical complexity can significantly increase compute time. Additionally, it suggests that this technique can be more widely applied to a range of different rocket bodies and box-wing spacecraft.

A key drawback of this technique is that due to the huge number of possible input combinations, it is not trivial to examine each combination individually to ensure that the input parameter set that minimised an RMSE measurement is in fact a unique solution. This drawback could possibly be addressed by developing a technique that incorporates additional metrics for quantifying the quality of the fit, and more rigorously examining the solution space.

It has also been shown in this paper that it may be possible to improve the fit between the real and synthetic data by increasing the complexity of the geometry model or by introducing additional zones of the geometry model that have unique BRDF parameters. However, this would result in a significant increase in the simulation run time to a point where a brute force technique is no longer feasible. This could be addressed by switching to a technique that does not require all possible combinations of input parameters to be tested, such as a genetic algorithm. These are the areas of future exploration for this work.

5. REFERENCES

[1] Robert L. Cook and Kenneth E. Torrance. A Reflectance Model for Computer Graphics. *ACM Transactions on Graphics (TOG)*, 1(1):7–24, 1982.

[2] J. Goguen, J. Veverka, J. L. Elliot, and C. Church. The lightcurve and rotation period of asteroid 139 Juewa. *Icarus*, 29(1):137–142, 1976.

[3] S Karpov, G Beskin, A Biryukov, S Bondar, E Ivanov, E Katkova, A Perkov, and V Sasyuk. Mini-Mega-TORTORA wide-field monitoring system with sub-second temporal resolution: first year of operation. *IV Workshop on Robotic Autonomous Observatories (Eds. María Dolores Caballero-García*, 48:91–96, 2016.

[4] Hugh G. Lewis, Graham G. Swinerd, Rebecca J. Newland, and Arrun Saunders. Active removal study for on-orbit debris using damage. *European Space Agency, (Special Publication) ESA SP*, 672 SP(April), 2009.

[5] J. C. Liou and N. L. Johnson. Collision activities in the future orbital debris environment. *Advances in Space Research*, 38(9):2102–2106, 2006.

[6] J. C. Liou and Nicholas L. Johnson. A sensitivity study of the effectiveness of active debris removal in LEO. *Acta Astronautica*, 64(2-3):236–243, 2009.

[7] Fabrizio Piergentili, Fabio Santoni, and Patrick Seitzer. Attitude Determination of Orbiting Objects from Lightcurve Measurements. *IEEE Transactions on Aerospace and Electronic Systems*, 53(1):81–90, 2017.

[8] Thomas Schildknecht, Jiri Silha, Jean-Noël Pittet, and Abdul Rachman. Attitude States of Space Debris Determined from Optical Light Curve Measurements. *Proc. of the 1st IAA Conference on Space Situational Awareness*, (1):2–7, 2017.

[9] Minghe Shan, Jian Guo, and Eberhard Gill. Review and comparison of active space debris capturing and removal methods. *Progress in Aerospace Sciences*, 80:18–32, 2016.

[10] Jiri Silha, T. Schildknecht, J. N. Pittet, D. G. Kirchner, M. Steindorfer, D. Kucharski, D. Cerutti-Maori, J. Rosebrock, S. Sommer, L. Leushacke, P. Karrang, R. Kanzler, and H. Krag. Debris attitude motion measurements and modelling by combining different observation techniques. *JBIS - Journal of the British Interplanetary Society*, 70(2-4):52–62, 2017.

[11] Charles J. Wetterer and Moriba Jah. Attitude estimation from light curves. *Journal of Guidance, Control, and Dynamics*, 32(5):1648–1651, 2009.